Chapter 5

Multiple-Input Multiple-Output Dual-band Dual-Circularly Polarized SIW Cavity-Backed Slot Antenna for Satellite and 5G Systems

5.1 Introduction

MIMO technology is a comprehensive approach that employs multiple transmit and receive antennas to increase the capacity of a wireless communication system within a given bandwidth. In other words, MIMO technology makes use of a solution that allows a communication system to transmit and receive several independent channels at the same time over the same wireless connection (and same frequency band), utilising multiple antenna topologies with no additional radiation power consumption. In order to meet the demands for high data rates, millimetre wave (mmWave) radio fre-

quency bands have been considered in the fifth-generation (5G) communication systems. Due to the substantial path loss and atmospheric absorption at mmWave, a single antenna element can not resist the attenuation [110]. To use the Multiple-Input Multiple-Output (MIMO) technology, the wireless system will have multiple antennas at both the sending and receiving ends. To satisfy the higher data rate and larger channel capacity requirements in wireless applications, wireless communication technology is rapidly transitioning from a single antenna system to multiple antenna (MIMO) systems.

For MIMO antenna systems to achieve maximum channel capacity, it is essential that the communication channels between the sender and receiver are completely uncorrelated. Therefore, numerous radiators at the transmitter and receiver ends must operate independently. The coupling inside the antenna's structure is one of the two primary factors that enhance channel correlation. This characteristic (actually its inverse) is known as antenna isolation, and it can be determined using the antenna's S-parameters. Even if the radiating components are well-isolated, the peculiarities of the antenna's radiation pattern can enhance channel correlation. This factor can be assessed using the antennas' correlation coefficients. MIMO technology includes two distinct features. First, MIMO enables a larger data rate by streaming independent data in parallel over the same channel. This method is known as spatial multiplexing [174]. The second factor is diversity, which is especially beneficial in combating fading. Furthermore, designing a multiband MIMO antenna is difficult since the isolation approach used for one operating band usually does not function at other frequencies. One of the most significant design features of a MIMO antenna is the design of an appropriate isolation network. Increasing the distance between ports reduces the coupling between the ports, but at the cost of the size of the antenna. In this chapter, a simple cavity-backed SIW based 2×1 MIMO antenna with an asymmetric cross-slot (AXS) to obtain dual-band dual-circularly polarized (DB-DCP) operation is proposed support satellite

and 5G cellular communications.

5.2 Antenna Configuration and Design

The top view of the proposed DB-DCP SIW based MIMO antenna is shown in Fig. 5.1(a). As can be seen, the proposed antenna of size $W_{gnd}\times L_{gnd}$ is printed on 1.57 mm thick RT-Duroid 5880 (ε_r=2.2 and tanδ=0.0009), having metallic ground plane on the bottom side. The SIW cavity of dimensions $W_{cav}\times L_{cav}$ is implemented using metal-filled vias (diameter d and pitch p) drilled inside all four sides of the substrate used along with conventional TE_{210} mode distribution. To ensure the minimum leakage of energy from the SIW cavity, $\frac{d}{p}\geq$ 0.5 and $\frac{d}{\lambda_o}\leq$ 0.1 are chosen [175]. A similar type of design has been reported in X-band for diplexing applications [89]. The eigenmode resonating frequencies propagating inside the SIW cavity having ε and μ as substrate permittivity and permeability, respectively, can be calculated as follows [176]:

$$f_{mnp} = \frac{1}{2\sqrt{\varepsilon\mu}}\sqrt{(\frac{m}{W_{cav,eff}})^2 + (\frac{n}{L_{cav,eff}})^2 + (\frac{p}{c})^2} \tag{5.1a}$$

$$L_{cav,eff} = L_{cav} - 1.08\frac{d^2}{p} + 0.1\frac{d^2}{L_{cav}} \tag{5.1b}$$

$$W_{cav,eff} = W_{cav} - 1.08\frac{d^2}{p} + 0.1\frac{d^2}{W_{cav}} \tag{5.1c}$$

where the standing wave pattern variations in the x-, y- and z-directions are referred by m, n, and p, respectively.

An array of metallic vias are made along L_{gnd}, which divides it into two equal sub-cavities, both excited with the help of 50Ω coaxial ports. These horizontally placed metallic vias prevent the spilling of electromagnetic waves of one port over other. The locations of these ports (i.e., F_H and F_V) are optimized for proper impedance matching. As a radiator, an AXS is etched from the center of the top layer of the SIW cavity and placed equally inside each cavity. Unlike symmetric slots [177], the AXS has unequal

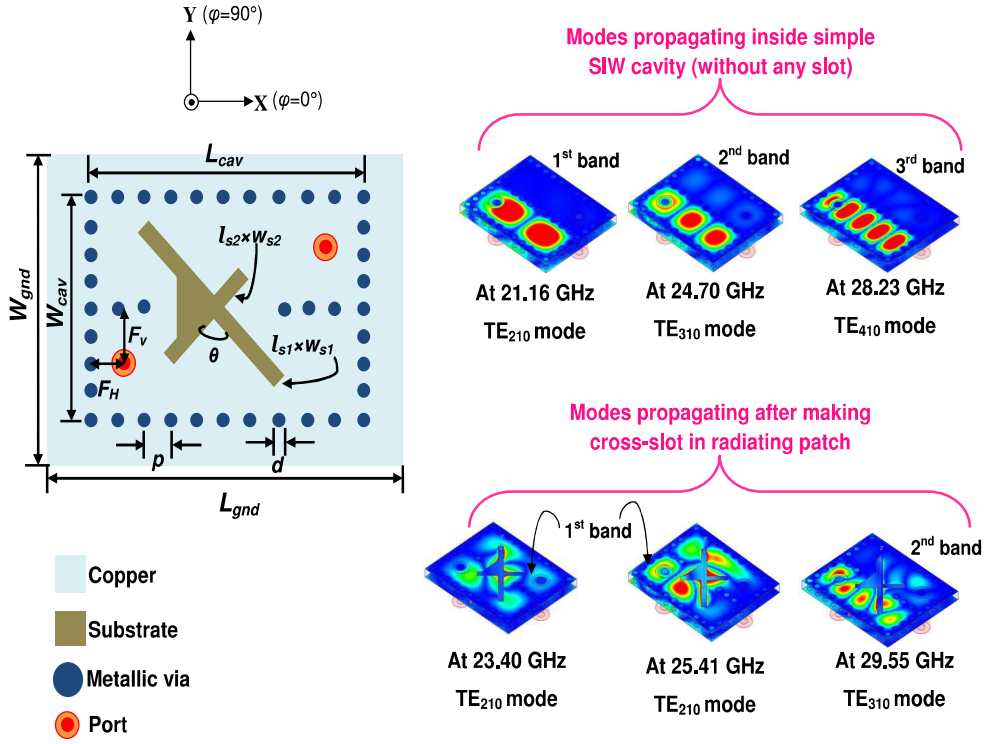

(a)

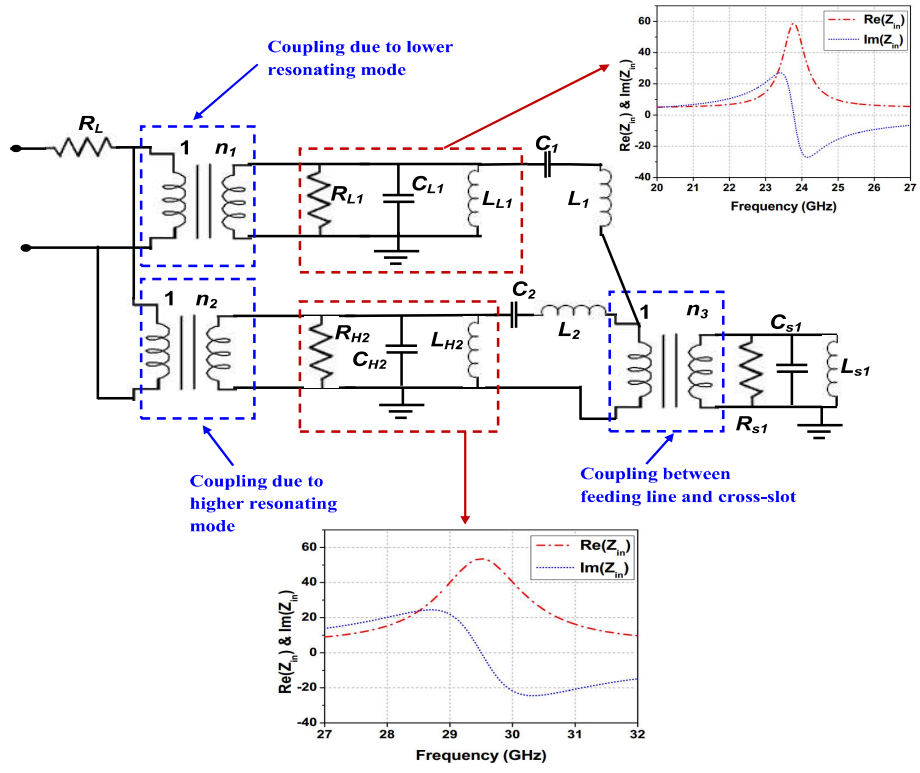

(b)

Figure 5.1: (a) Schematic of the proposed antenna design showing cavity modes without and with AXS at resonating frequencies when only port-1 is excited and (b) equivalent circuit of the proposed antenna.

arm lengths making an angle of θ=90° with each other and 45° with the symmetric axis. The field distribution of the modes propagating inside both SIW cavities before and after the etching slot (when excited by either port) is shown in Fig. 5.1(a). The final optimized dimensions of the proposed antenna are W_{gnd}=22, L_{gnd}=26, W_{cav}=16, L_{cav}=20, p=1, d=0.5, l_{s1}=17, l_{s2}=9, w_{s1}=w_{s2}=1, θ=90°, F_H=3.5 and F_V=4 (units: millimeters). The average value of the conductor losses (α_{ohmic}), dielectric losses (α_{diel}), radiation losses (α_{rad}) are 6.1 dB, 4.06 dB, and 16 dB respectively within the range of operating frequency.

5.3 Equivalent Circuit Analysis

To analyse the interaction between the propagation modes inside the SIW cavity with AXS, the equivalent circuits model of the proposed MIMO antenna, is studied. Here, the modes propagating inside the SIW cavities can be seen as a parallel combination of RLC resonant circuit where R_{L1}, L_{L1}, C_{L1} and R_{H2}, L_{H2}, C_{H2} correspond to the resonating modes propagating at lower and higher frequencies, respectively (i.e., 23.40 GHz and 29.55 GHz). The values of various R, L, C components as shown in Fig. 5.1(b) corresponding to both lower and higher resonating frequencies and coupling with AXS are extracted using single port analysis in ANSYS HFSS. A small series resistance R_L(=4.68Ω) is also included in the proposed MIMO antenna equivalent circuit to account for the inherent losses of coaxial-line. Furthermore, the AXS etched at the top of the SIW cavity can also be modeled as a parallel combination of the RLC circuit. After calculating the optimum values of equivalent circuit elements for each resonating mode and AXS separately, these models are combined with the help of three ideal transformers (with turn-ratio 1:n_1/n_2/n_3) to design the equivalent circuit for the proposed dual-band antenna. The loading effect between the resonating modes, a Tee network consisting of series inductor and capacitor are introduced in each branch of the equivalent circuit. The optimized values of each element of the equivalent circuit are

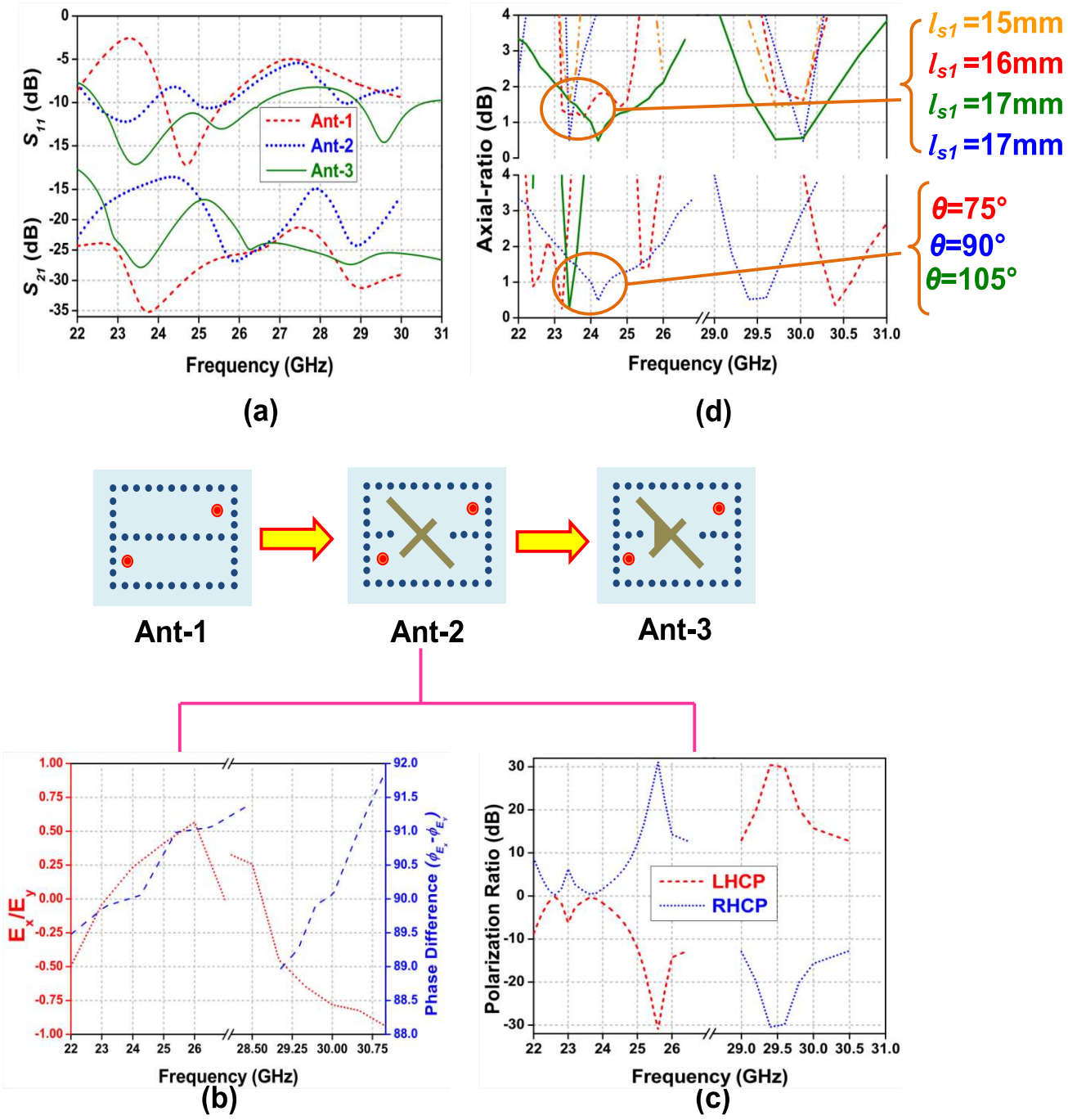

Figure 5.2: Design steps followed to design proposed antenna (a) S_{11}/S_{21} of different stages, (b) $|\frac{E_X}{E_Y}|/\angle E_X - \angle E_Y$ and (c) PCR for Ant-2 and (d) parametric study for different values of l_{s1} and θ.

as follows: n_1=39.67, n_2=43.67, R_{L1}= 85.23Ω, L_{L1}= 18.01 nH, C_{L1}= 2.488 fF, R_{H2}= 93.23Ω, L_{H2}= 27.72 nH, and C_{H2}= 1.05 fF.

5.4 Design Steps and Parametric Study

The design stages of the proposed SIW based MIMO antenna, along with S-parameters of each stage, are illustrated in Fig. 5.2. The detailed description of each design step is outlined in the following points:

1. To facilitate the MIMO configuration, the original SIW cavity is divided into two sub-cavities partitioned with the help of a row of metallic vias. Three resonant modes, i.e., TE_{210}, TE_{310}, and TE_{410} propagating at 21.16, 24.70, and 28.23 GHz, respectively, within the cavity are shown in Fig. 5.1(a). Fig. 5.2(a) shows a good level of isolation (27 dB on average) between the excitation ports.
2. Next, an AXS is etched on the top of the SIW cavity, as shown in Fig. 5.2 as Ant-2. The AXS is etched on top of the SIW cavity by removing a few metallic vias of the row separating the lower and upper sub-cavities. The AXS loading disturbs the current path of dominant TE_{210} mode and brings resonance shift from 21.16 GHz to 23.40 GHz and 24.70 GHz to 25.41 GHz. The superposition of modes (TE_{210} and TE_{310}) in the lower frequency band produces large IBW and leads to the generation of hybrid modes, as shown in Fig. 5.1(a) (strong current density near AXS arms). The angle θ and arm lengths of the AXS help in obtaining orthogonal E-field components having almost equal amplitudes, i.e., $|\frac{E_X}{E_Y}| \approx 1$ and phase difference, PD=$\angle E_X - \angle E_Y = 90°$. Fig. 5.2(b) illustrates the amplitude ratio and PD fluctuations for Ant-2. It is observed that the amplitude ratio varies from -0.49 to 0.57 and -0.94 to 0.33 in lower and upper-frequency bands, respectively. Also, the PD varies from 89.47° to 91.36° and 88.97° to 91.88° in lower and upper-frequency bands, respectively. Fig. 5.2(c) shows the polarization-ratio of Ant-2 where right-handed CP (RHCP) in first and left-handed CP (LHCP) in the second operating frequency band are observed. Removing few metallic vias for etching the AXS degrades the isolation between the excitation ports, i.e., from 27 dB to 19 dB, on average.

3. To improve the isolation between the excitation ports, the AXS junction is widened, shown as Ant-3 in Fig. 5.2. Here, an improvement of about 6 dB in isolation compared to Ant-2 is observed. A parametric study to better understand the effect of AXS dimensions (l_{s1} and θ) on ARBW is conducted, which is shown graphically in Fig. 5.2(d), where it is evidently shown that 3 dB ARBW within the first operating frequency band varies from 8.67% to 2.13% when l_{s1} goes from 15 mm to 18 mm and 4.81% to 1.92% when θ varies from 75° to 105°. For the second band, the ARBW varies from 1.07% to 0.93% and 3.59% to 0% with a similar variation in l_{s1} and θ, respectively. No DB-DCP beyond l_{s1}=18.2 mm, and θ=95° is seen. The surface current distribution at 23.77 and 29.50 GHz, as shown in Fig. 5.3, illustrates the RHCP and LHCP behavior of the proposed antenna within lower and upper operating frequency bands.

5.4.1 Matching characteristics

The simulated and measured S_{11} and S_{21} of the proposed DB-DCP antenna are shown in Fig. 5.4(b). When excited with port-1 only, the proposed antenna shows measured IBW ranging from 22.60-26.36 GHz (15.36%; Band-I) and 29.04-30.42 GHz (4.64%; Band-II), which are little deviated from the simulated value of 22.49-26.61 GHz (16.78%) and 28.90-30.61 GHz (5.75%) due to fabrication errors. Tolerances for simulated vs. experimental resonating frequencies of the proposed antenna are ±0.92% at 23.7 GHz and ±0.06% at 29.5 GHz. Last but not least, the simulated/measured port isolation is better than 15 dB and 25 dB in Band-I and Band-II, respectively.

5.5 Results and discussion

The proposed DB-DCP MIMO SIW antenna has been fabricated using a printed circuit board process and tested. The scattering parameters and radiation characteristics were measured using Agilent vector network analyzer N5247A and inside anechoic-chamber,

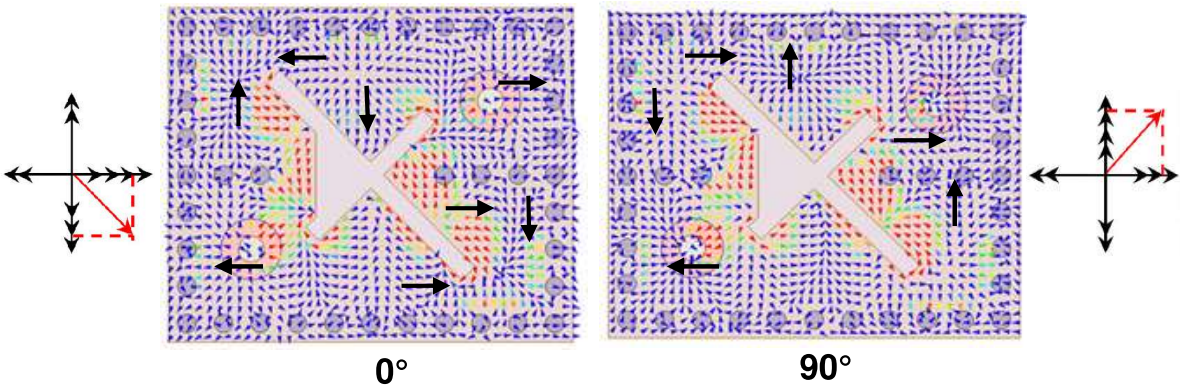

(a)

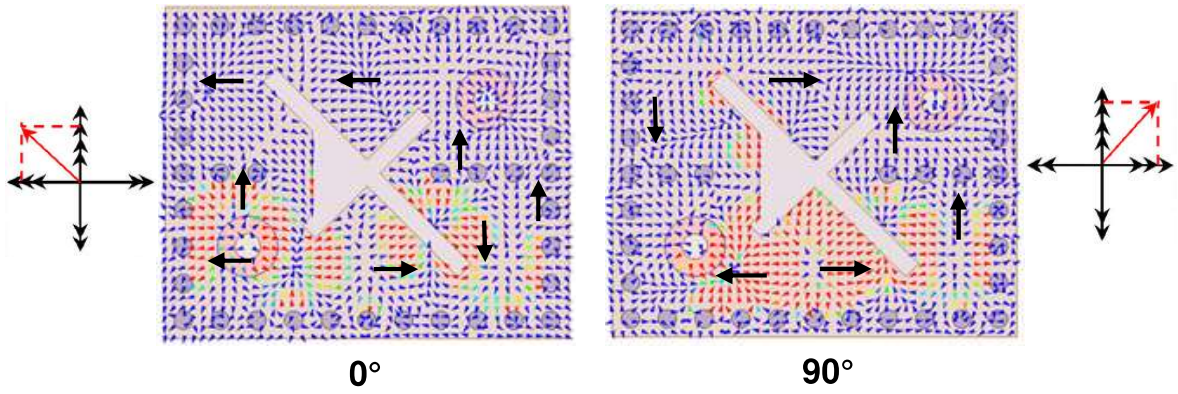

(b)

Figure 5.3: Surface current density of the proposed antenna showing (a) RHCP behavior at 23.77 GHz, and (b) LHCP behavior at 29.50 GHz.

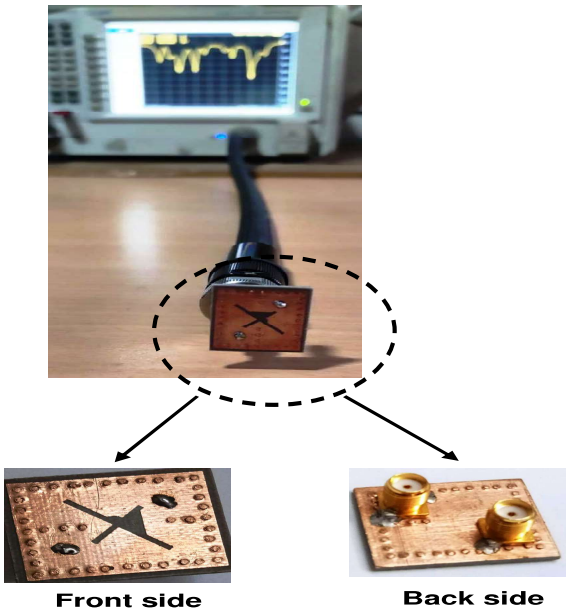

(a)

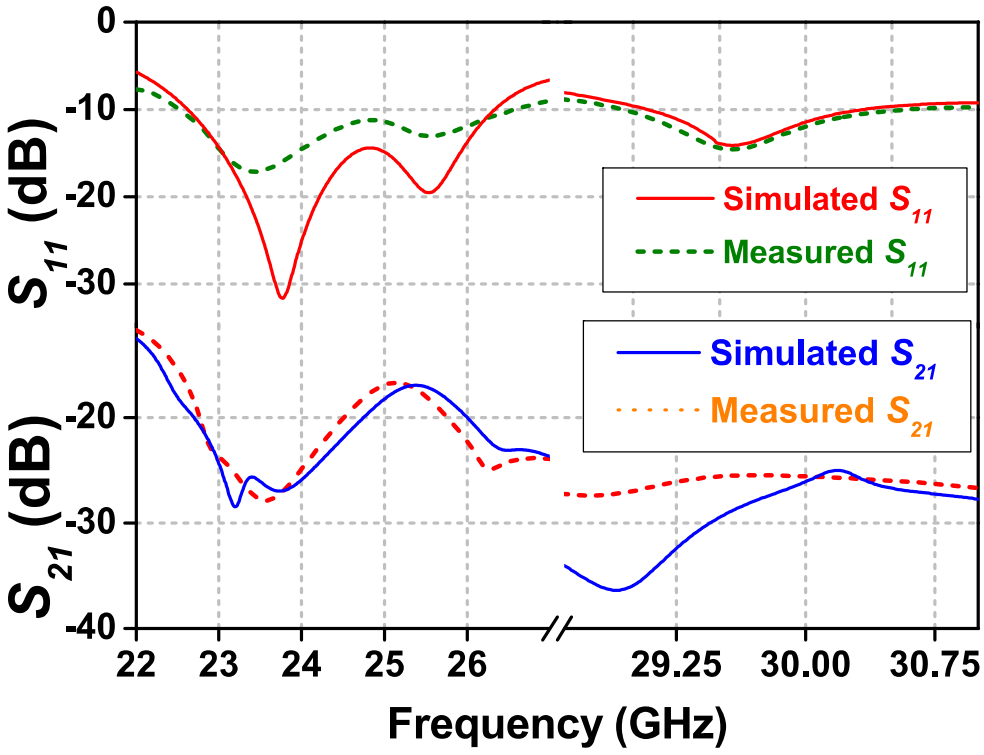

(b)

Figure 5.4: Matching characteristics of the proposed antenna (a) Proposed antenna while testing with VNA, and (b) Simulated vs. measured S_{11}/S_{21} (in dB).

respectively. The fabricated version of the proposed antenna while testing with VNA is shown in Fig. 5.4(a).

5.5.1 Radiation characteristics

Fig. 5.5(a) shows the simulated and measured peak gain and FBR of the proposed DB-DCP MIMO antenna. When excited with port-1 only, the antenna has a measured peak gain of 12.47 dBic and 7.71 dBic in Band-I and II, respectively, and having an average FBR of more than 20 dB in both frequency bands. The measured peak gain is slightly lower than the simulated results in each frequency band due to errors during the fabrication process. Fig. 5.5(b) shows the proposed antenna simulated and measured axial-ratio when exited with port-1 only. The proposed antenna has a measured 3 dB ARBW ranging from 22.62-26.33 GHz (15.16%) and 29.20-30.12 GHz (3.10%) in Band-I and II, respectively, agrees well with the simulated AR curve. A minimum axial-ratio of 0.48 and 0.52 dB is reached within Band-I and Band-II, respectively. The ARBW in both operating frequency bands lies completely within the impedance bandwidth range. The 2D radiation patterns at 23.77 and 29.5 GHz in E-plane (ϕ=0°) and H-plane (ϕ=90°) are displayed in Fig. 5.6(a)-5.6(d).

5.5.2 Diversity performance

To comprehend the diversity performance of the proposed MIMO antenna, the following different parameters are calculated. For simplicity, these parameters can be calculated using S-parameters. Envelope correlation coefficient (ECC) is a figure-of-merit which demonstrates the correlation between the MIMO antenna elements when receiving the signals simultaneously [178]. ECC can be calculated either using S-parameters or far-fields [179]. Similarly, diversity gain (DG) describes the overall gain enhancement of a MIMO antenna system over a time-averaged signal-to-noise ratio. Fig. 5.7 shows ECC calculated using S-parameters or far-fields. The simulated and measured ECC and

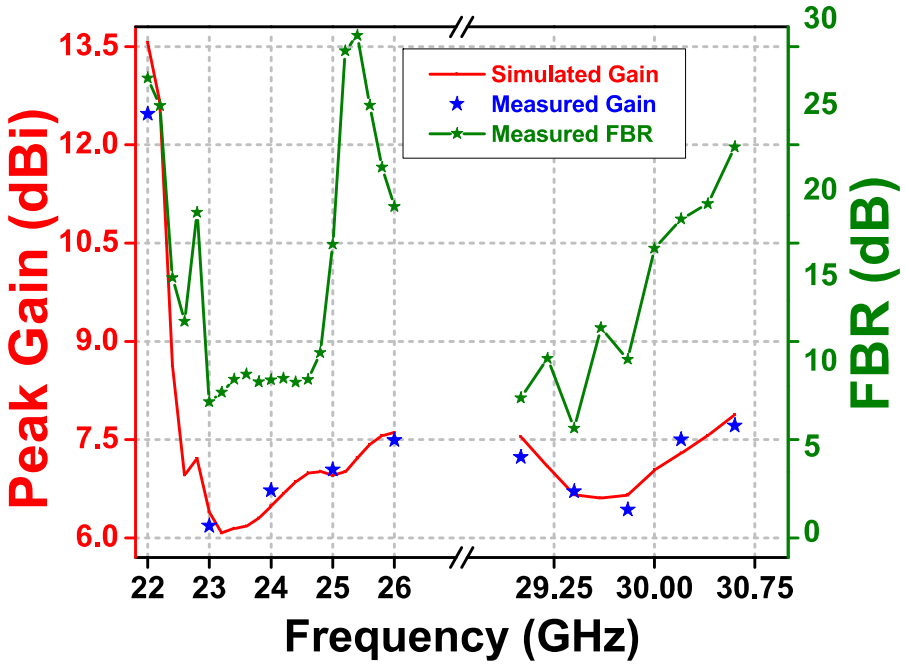

(a)

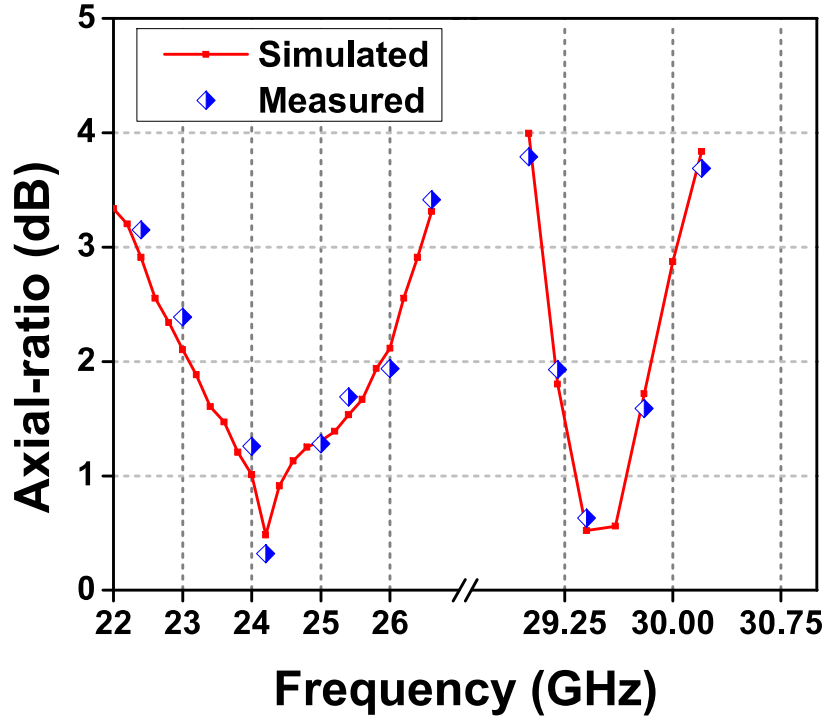

(b)

Figure 5.5: Radiation characteristics of the proposed antenna showing simulated and measured peak gain/FBR.

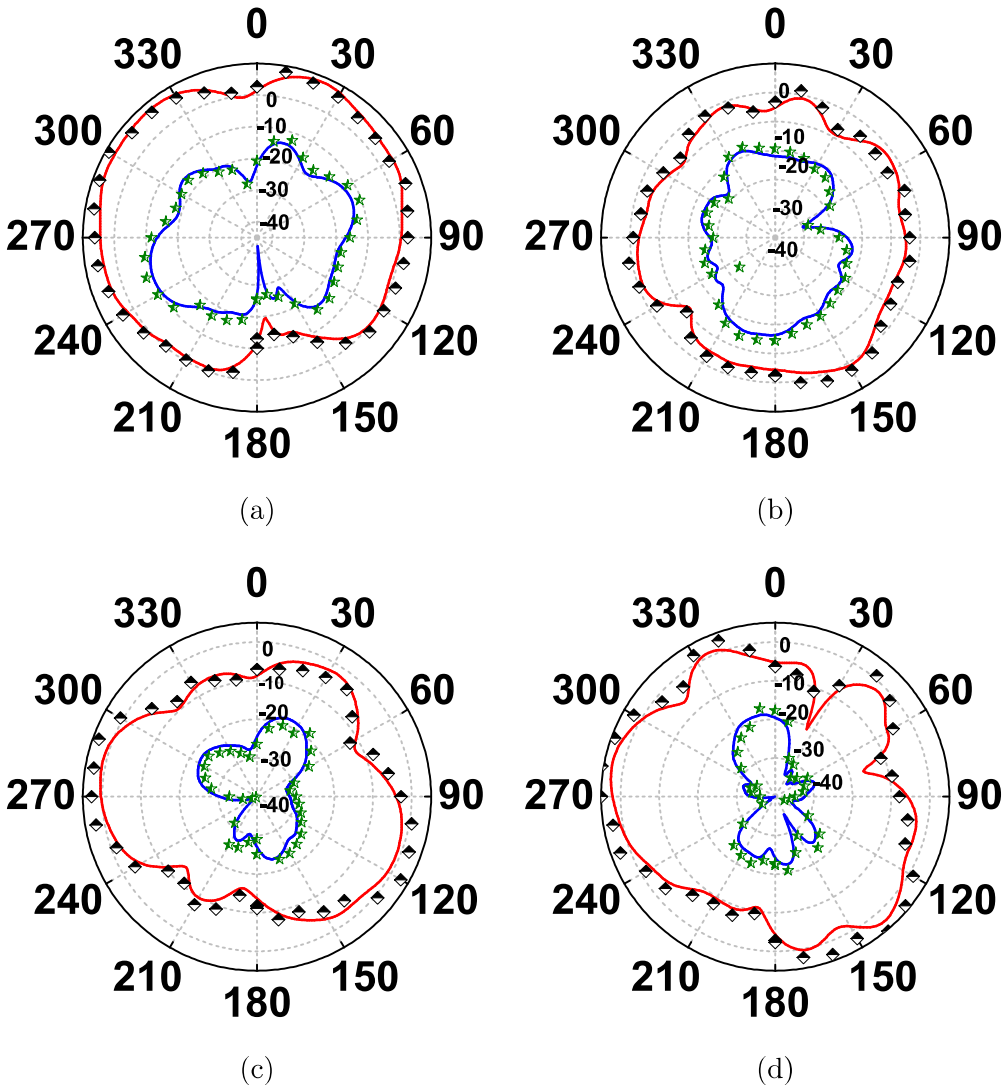

Figure 5.6: Radiation characteristics of the proposed antenna showing simulated and measured (a) & (b) E/H-plane radiation patterns at 23.77 GHz, and (c) & (d) E/H-plane radiation patterns at 29.5 GHz —Simulated co-pol - - measured co-pol —simulated x-pol - - measured x-pol

DG for the proposed MIMO antenna as computed using equations given in [178] are plotted in Fig. 5.8. It confirms that both simulated and measured results are in good agreement, indicating desirable MIMO performance. In the present case, the measured ECC < 0.004 and DG > 9.998 are obtained within the operating frequency bands, which fall within acceptable limits. In our work, the measured ECC is about 87% better than the closely spaced SIW based MIMO antenna discussed in [180]. Assuming

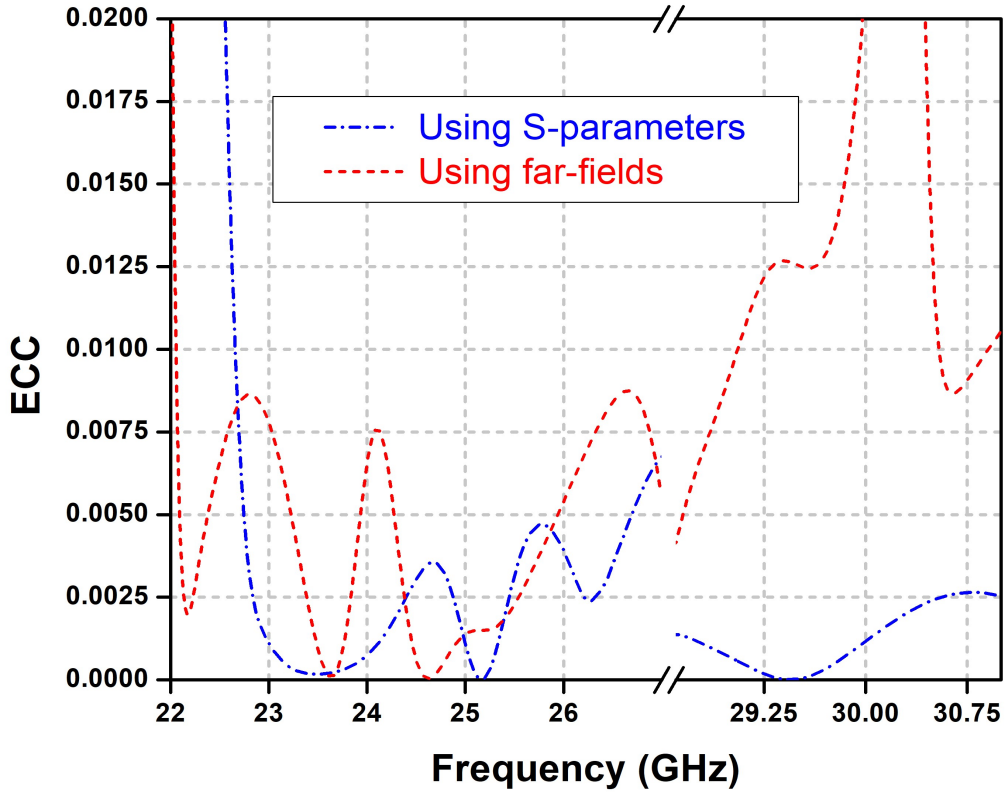

Figure 5.7: Comparison of ECC calculated using S-parameters and far-fields.

the uniformly distributed incoming signals and lossless MIMO antenna elements, the ECC and DG for the MIMO antenna elements can be determined using the following equations [178]

$$\rho_e(i,j,N) = \frac{|\sum_{n=1}^{N} S_{i,n}^{*} S_{n,j}|^2}{\prod_{k=(i,j)}(1-\sum_{n=1}^{N} S_{i,n}^{*} S_{n,j})} \tag{5.2a}$$

$$\rho_e(i,j,N) = \frac{\int\int_{4\pi} \vec{E}_1(\theta,\phi).\vec{E}_2^{*}(\theta,\phi)d\Omega}{\sqrt{\int\int_{4\pi} \vec{E}_1(\theta,\phi).\vec{E}_1^{*}(\theta,\phi)d\Omega \int\int_{4\pi} \vec{E}_2(\theta,\phi).\vec{E}_2^{*}(\theta,\phi)d\Omega}} \tag{5.2b}$$

where $\vec{E}_1$ and $\vec{E}_2$ are the individual far-field radiation patterns produced when excited with port-1 and port-2, respectively.

$$DG = 10\sqrt{1-|\rho_{i,j}|^2} \tag{5.3}$$

Another diversity performance parameter known as mean effective gain (MEG) is

used to compute the average signal strength received by each MIMO antenna element. It can be defined as the ratio of the signal received by any two antenna elements (or power imbalance) is one (or 0 dB), i.e., $|\frac{MEG_i}{MEG_j}| \approx 1$, calculated using (5.4). Also, the correlation between the MIMO elements leads to a reduction in MIMO capacity [181]. Hence, a parameter known as channel capacity loss (CCL) is calculated using (5.5) [179].

$$MEG_i = 0.5\eta_{i,rad} = 0.5[1 - \sum_{j=1}^{M} |S_{ij}|^2] \tag{5.4}$$

$$CCL = -log_2|\rho_{1,1}\rho_{2,2} - \rho_{1,2}\rho_{2,1}| \tag{5.5}$$

where $\rho_{1,1} = (1 - |S_{11}|^2 - |S_{12}|^2)$, $\rho_{2,2} = (1 - |S_{22}|^2 - |S_{22}|^2)$, $\rho_{1,2} = (S_{11}^* S_{12} + S_{21}^* S_{22})$ and $\rho_{2,1} = (S_{22}^* S_{21} + S_{12}^* S_{11})$.

Fig. 5.8(b) shows that the proposed antenna achieves CCL lower than 0.31 and 0.18 with a minimum value of 0.003 and 0.01 in Band-I and II, respectively (which is 5.26% better than the MIMO configuration discussed in [118]). Similarly, MEG is within Band-I and II varies from -0.2 dB to 0.241 dB and -0.8 dB to 0.245 dB, respectively.

Table 5.1: comparison between proposed DB-DCP MIMO antenna with other works

Reference No.	f_r (GHz)	Size (mm^2)	IBW (%)	ARBW (%)	Polarization state	Peak Gain (dBic)	MIMO features	Technique used
[123]	28	48×31	17.54	-	Linear	10	Yes	CLL monopole array
[124]	30	48×21	5.80	-	Linear	>7	Yes	DRA
[125]	28	30×30	7.14	-	Linear	6.1	Yes	Monopole
[126]	27/39	26×11	14.81/12.98	-	Linear	5/5.7	Yes	Monopole
[182]	28	70×63.50	5.66	4.60	LHCP	13.09	No	Multilayer SIW
[183]	37/47	-	1.1/1.4	1.1/1.5	Dual	5/5.7	No	SIW+Annular slot
[184]	28/33/38	30×15	3.7/2.3/3.1	1.2/-/0.8	Dual	6.96/8/9.41	No	SIW+Circular slot
[185]	12.24	22.5×22.06	4.2	1.6	LHCP	7.4	No	SIW+Elliptical slot
[186]	28/38	19.8×12.4	5.37/3.93	-/6.81	Dual	8.17 (avg.)	Yes	Leaf-like array
Proposed antenna	**23/29**	**26×22**	**15.36/4.64**	**15.16/3.10**	**Dual**	**12.47/7.71**	**Yes**	**SIW+AXS**

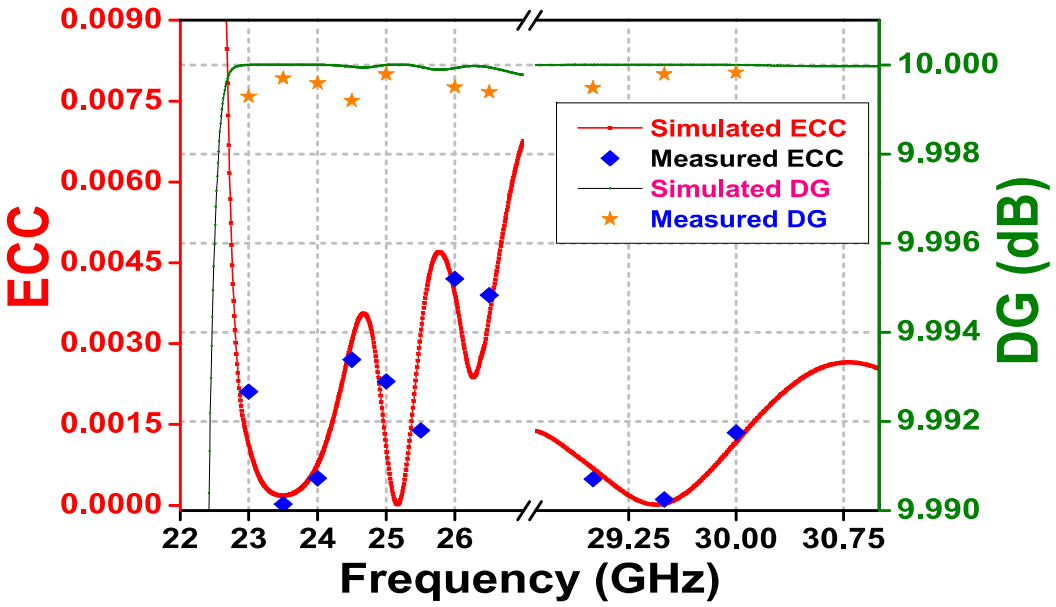

(a)

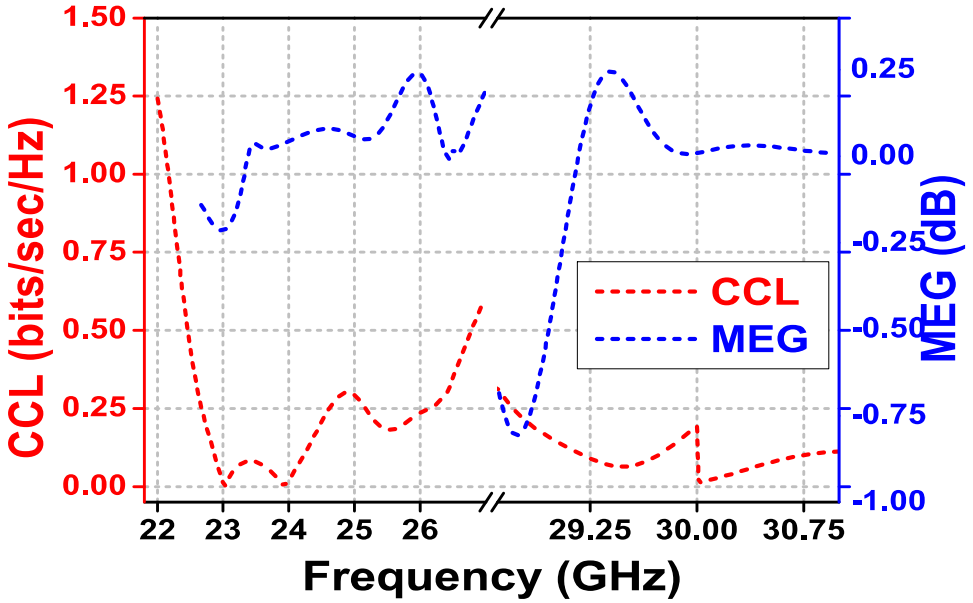

(b)

Figure 5.8: Simulated and measured diversity parameters of the proposed antenna (a) ECC/DG and (b) CCL/MEG.

5.6 State-of-the-art Comparison

Compared to existing antennas, the proposed work has several advantages, including:

1. Thanks to the structure reuse in the proposed antenna design, where the whole SIW cavity is partitioned into two sub-cavities. This helps in maintaining the compact size, facilitating the easy integration with 5G user equipment as compared to other MIMO antennas [123–125, 182–184].
2. The partitioning using metallic vias offers the compact size for diversity performance and provides good isolation between the excitation ports without using any decoupling structure.
3. The proposed antenna shows dual sense of polarization while ARBW lies completely within the IBW and covers 98.70% and 66.81% of IBW in frequency Band-I and II, respectively. Also, it shows better performance in terms of IBW [124–126, 182–186] and gain [123–126, 183–186].
4. The proposed antenna shows good diversity characteristics with ECC, DG, CCL and $|\frac{MEG_i}{MEG_j}|$ within their acceptable limit, i.e., $\ll$0.5, $\gg$9.99, $\leq$0.4 bits/sec/Hz and 1 (or 0 dB), respectively, which make it a suitable candidate for satellite and 5G cellular communications.

In this chapter, a dual-band dual-polarized SIW based CP MIMO antenna with potential use for satellite communications and 5G application has been presented and realized on RT-Duroid 5880 substrate with overall dimension of 22×18 mm^2. To achieve CP in both operating frequency bands, the arms of the AXS was tuned sufficiently to realize 3 dB ARBW from 22.62-26.33 GHz and 29.20-30.12 GHz within the IBW ranging from 22.60-26.36 GHz (Band-I) and 29.04-30.42 GHz (Band-II), respectively. A measured average gain of 7.52 dBic and 7.15 dBic has been obtained in Band-I and II, respectively. Both MIMO ports have more than 28 dB isolation and FTBR of more than 20 dB, on average, in both operating frequency bands. Moreover, the proposed antenna has been accomplished with good radiation patterns and diversity

performance and both operating frequency bands can feasibly support satellite and 5G cellular communications. In the upcoming chapter, the major contributions made in the thesis, conclusion drawn during the whole investigation and future scope are summarized.